Shear melting of silicon and diamond and the disappearance of the polyamorphic transition under shear

Gianpietro Moras,[1,*] Andreas Klemenz,[1] Thomas Reichenbach,[1] Adrien Gola,[2]
Hiroshi Uetsuka,[3] Michael Moseler,[1,4] and Lars Pastewka[1,2]

[1]*Fraunhofer IWM, MicroTribology Center μTC, Wöhlerstraße 11, 79108 Freiburg, Germany*
[2]*Department of Microsystems Engineering, University of Freiburg, Georges-Köhler-Allee 103, 79110 Freiburg, Germany and Institute for Applied Materials, Karlsruhe Institute of Technology, Straße am Forum 7, 76131 Karlsruhe, Germany*
[3]*Asahi Diamond Industrial Co. Ltd., 787 Tabi, Ichihara Chiba, 290-0515, Japan*
[4]*Institute of Physics, University of Freiburg, Hermann-Herder-Straße 3, 79104 Freiburg, Germany*

(Received 29 August 2017; revised manuscript received 9 March 2018; published 3 August 2018)

Molecular dynamics simulations of diamond-cubic silicon and carbon under combined shear and compression show the formation of an amorphous solid with liquidlike structure at room temperature. Consistent with the opposite density changes of the two crystals upon melting, the amorphous material is denser than the crystal in silicon and less dense than the crystal in carbon. As a result, its rate of formation is enhanced by pressure in silicon but suppressed in carbon. These results are particularly unexpected for silicon, whose amorphous structure is supposed to be liquidlike only when hydrostatically compressed above the polyamorphic transition pressure (∼14 GPa). Below this pressure, amorphous silicon is expected to have a low-density structure with density close to that of the diamond-cubic crystal. Our simulations show that this polyamorphic transition disappears under shear and high-density, liquidlike amorphous silicon with metallic ductility forms even at low pressure. These results are potentially transferable to other diamond-cubic crystals, like germanium and ice I_h, and provide insights into nonequilibrium materials transformations that govern friction and wear in tribological systems.

DOI: 10.1103/PhysRevMaterials.2.083601

I. INTRODUCTION

Crystalline materials can respond to shear stress by undergoing localized plastic deformation. While in metals this typically occurs through the motion of dislocations [1], brittle covalent crystals with a comparatively low dislocation mobility can plastically deform through the formation of amorphous shear bands [2–5]. This class of materials includes tetrahedral crystals like silicon and diamond, whose behavior under combined compressive and shear stress is of high relevance in technology.

Amorphization of Si-I [diamond-cubic silicon, Fig. 1(a)] is responsible for nanoscale wear of silicon tips for atomic force microscopy [6–8] and affects the subsurface damage and surface quality of diamond-cut silicon crystals [9,10]. Contact loading experiments suggested that amorphous silicon (a-Si) forms upon unloading of the high-pressure, metallic Si-II [β-tin, Fig. 1(a)] phase [11]. Lately, however, a number of experimental and simulation works that focus on nanoscale plasticity have confirmed the existence of direct, shear-driven amorphization processes in Si-I crystals during, e.g., nanoindentation [12,13], scratching [9,14,15], shock compression [16], and uniaxial compression [2,17]. Yet, little is known about the physical process underlying the growth of the amorphous regions under shear strain, the response of this process to variations of normal pressure and shear rate, and the structure of the resulting a-Si. Density and structure of shear-induced a-Si are crucial because a-Si can exist in two significantly different polyamorphic forms [18] that determine its mechanical response to shear. Experiments showed that low-density amorphous Si (LDA-Si) transforms into high-density amorphous Si (HDA-Si) when hydrostatically compressed, with a nonequilibrium polyamorphic transition that occurs at about 14 GPa [18–20]. LDA-Si is a semiconductor with structure and density that are very close to those of Si-I, while HDA-Si is metallic and has structural features that are similar to those of Si-II and the liquid phase [18].

The process underlying shear-driven amorphization is better understood for diamond-cubic C, whose amorphous form (a-C) does not undergo a polyamorphic transition upon compression [Fig. 1(b)]. Molecular dynamics (MD) simulations of diamond polishing showed that an a-C region grows at the sliding interface between two diamond crystals in relative motion [5]. Amorphization was discovered to be a fully mechanical, nonequilibrium process that does not rely on temperature activation and progresses by erosion of the crystal during shear of the adjacent a-C.

In this article we show that shear-driven amorphization of Si-I and diamond are caused by equivalent mechanical processes. These processes lead to shear melting [21,22] as—even at room temperature—the resulting amorphous solids are structurally comparable to the liquid phases of silicon and diamond. Conversely, amorphous Si and C that are subjected to compression without shear have significantly different structures and densities [Figs. 1(c) and 1(d)]. In particular, shear-induced a-Si has a HDA-like structure even at pressures that are much lower than the polyamorphic transition, where

*gianpietro.moras@iwm.fraunhofer.de

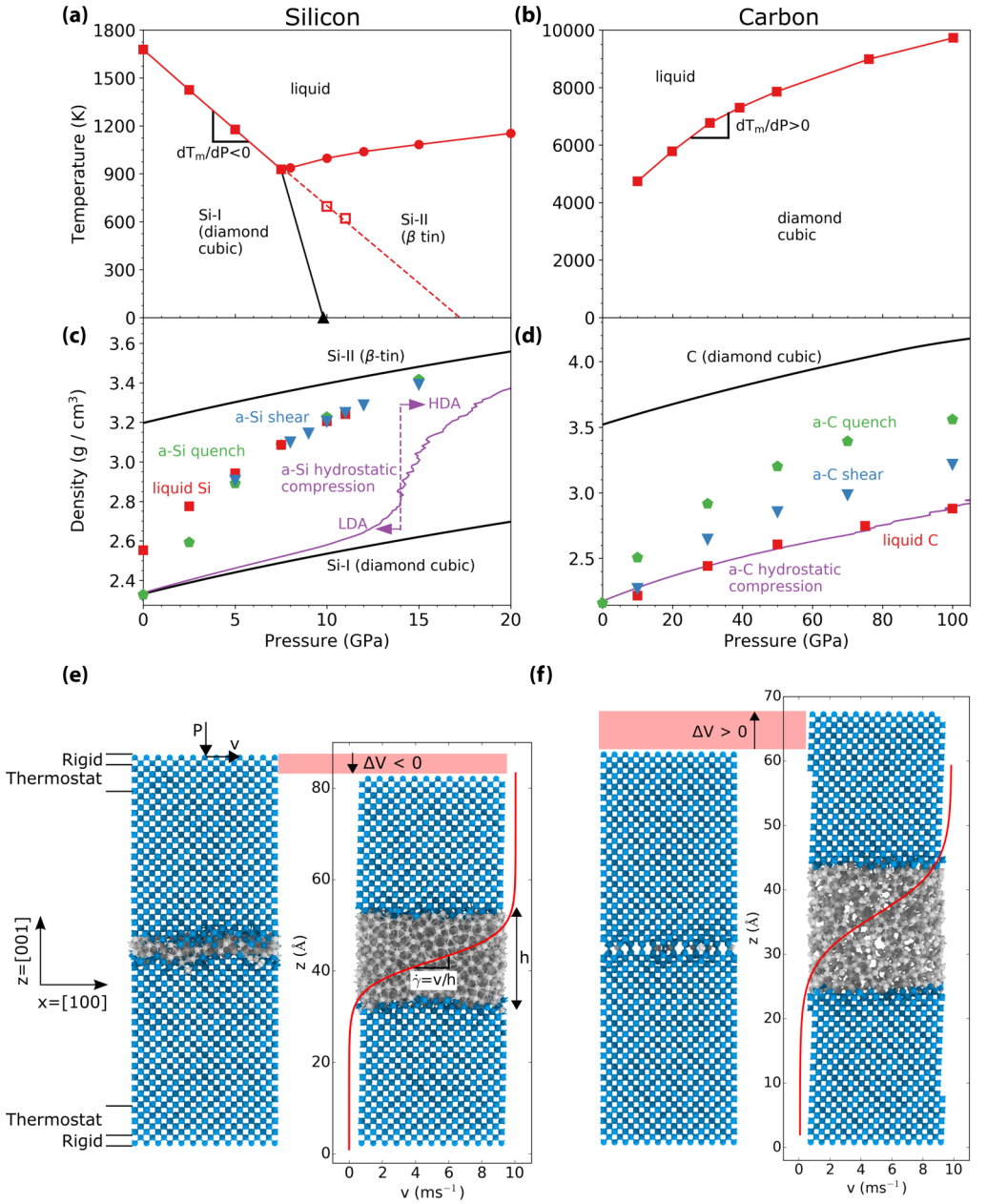

FIG. 1. (a), (b) P-T phase diagrams for Si (a) and C (b) in the pressure range of interest for the simulations presented in this work. The red symbols show the melting temperature $T_m(P)$ calculated in this work by MD simulations (see discussion S1 in the Supplemental Material [34]). Squares refer to the diamond-cubic phase of Si and C, and circles to Si-II, while the black triangle shows the Si-I/Si-II transition pressure at 0 K. Open squares in panel (a) represent transitions involving a metastable Si-I phase. Lines connect calculated data and are guides to the eye. (c), (d) Pressure dependencies of the density for different Si (c) and C (d) phases, as obtained by MD simulations (see discussion S2 in the Supplemental Material [34]). Black solid lines refer to crystalline phases, red squares to the liquid phases of panels (a), (b). The purple solid line indicates the density of an amorphous phase obtained initially at $P = 0$ and hydrostatically compressed. Blue and green symbols refer to amorphous samples obtained by shear-induced amorphization and quenching from the melt, respectively. (e) Snapshots from MD simulations of two Si-I crystals sliding against each other at a velocity of 10 m s^{-1} and 10 GPa normal load. The left snapshot is taken after pressure equilibration but before sliding, while the snapshot on the right is taken after 15 ns simulation time. Blue spheres are Si atoms in the Si-I phase, while gray spheres are Si atoms in an amorphous configuration. The red curve is an averaged velocity profile along x and shows a Couette-like profile. Analogous snapshots for diamond are depicted in panel (f). Note that the Si and C model systems have the same number of atoms but their size is scaled so that they have the same size along x in this figure. The volume variation upon amorphization is schematically shown as a variation of system height.

a-Si is expected to have a diamondlike LDA structure. As a result, the Clausius-Clapeyron relation for the liquid phases, which relates the density change upon melting to the slope of the melting line in the pressure-temperature (P-T) phase diagram [Figs. 1(a) and 1(b)] [23,24], is also valid for shear melting. Shear-induced a-Si is denser than Si-I while a-C is

less dense than diamond [Figs. 1(c) and 1(d)]. Since increasing the normal load during amorphization favors densification and suppresses volume expansion, the amorphization rates of Si and C show opposite sensitivity to changes in normal pressure.

II. RESULTS

To investigate the shear-driven formation of a-Si and to reexamine shear-driven formation of a-C, we follow the MD approach used in Ref. [5] for the amorphization of diamond. The atomic forces are calculated with screened versions [25] of the empirical bond-order potential developed by Kumagai *et al.* [26] for Si, and by Tersoff [27] for C. These potentials were chosen because they are simple but able to suitably describe elasticity, bond breaking, amorphization, and phase transitions [Figs. 1(a)–1(d)] in the two material systems [25]. For both Si-I and diamond, we consider two single crystals that slide against each other. Each single crystal is composed of 2592 atoms and is oriented along the cubic ⟨001⟩ directions, resulting in a $32.574 \times 32.574 \times 48.861\ \text{Å}^3$ Si-I crystal and a $21.396 \times 21.396 \times 32.094\ \text{Å}^3$ diamond crystal. The two blocks slide against each other along the [100] direction [Figs. 1(e) and 1(f)] and periodic boundary conditions are applied in the (001) sliding plane. We apply the normal pressure P using the pressure-coupling algorithm described in Ref. [28]. Once the system has reached the desired equilibrium pressure, we apply a constant sliding velocity to the top rigid group of atoms. The temperature of the system is controlled by the Galilean-invariant Peters thermostat [29] applied on two horizontal slices that are located close to the top and bottom rigid layers and far from the sliding interface [5]. The integration of the equations of motion is performed using the velocity-Verlet algorithm [30] with a time step of 0.5 and 0.1 fs for Si and C, respectively. Adatoms are placed on one of the sliding surfaces before pressure equilibration to nucleate amorphization.

We start by comparing sliding simulations of Si-I and diamond at the same normal pressure (10 GPa), temperature (300 K), and sliding velocity ($v = 10\ \text{m s}^{-1}$) used in Ref. [5]. After equilibration of Si-I at the target normal pressure and temperature, a thin disordered region consisting of about four atomic planes forms at the interface between the two Si crystals. Upon sliding, the thickness of the amorphous region grows continuously in time [Fig. 2(a)]. Analogous plots for C are shown in Ref. [5]. As amorphization progresses, the system volume decreases for Si-I [Fig. 1(e)] while it increases for C [Fig. 1(f)], indicating that the a-Si phase is denser than Si-I while a-C is less dense than diamond. Interestingly, in both materials the density of the amorphous material is about the same as that of the liquid phase at the melting point $T = T_\text{m}$ and $P = 10$ GPa [Figs. 1(c) and 1(d)]. For Si, this liquid is a high-density liquid (HDL) with a density comparable to that of Si-II [31–33].

A number of observations suggest that, like in C [5], the amorphization process in Si-I is mechanically driven. During shear, the temperature of the a-Si region remains considerably lower than T_m (typically lower than 330 K). The shear strain is entirely accommodated through the plastic deformation of the growing amorphous region of thickness h in which the velocity profile is Couette-like [Figs. 1(e) and 1(f)] with

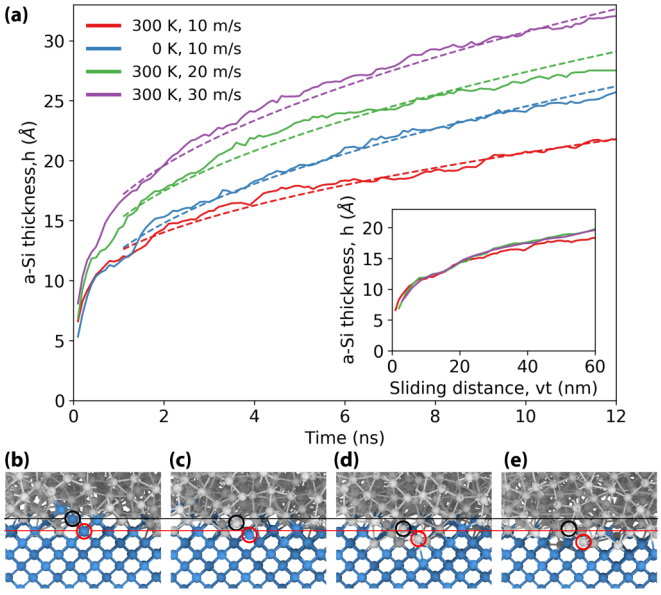

FIG. 2. (a) Time evolution of the a-Si region thickness h (solid lines) and square root fitting functions [dashed lines, Eq. (1)] for the temperature/velocity combinations indicated in the legend and 10 GPa normal pressure. The inset shows the evolution of h as a function of the sliding distance vt for the simulations at 300 K. (b)–(e) Snapshots of the a/c interface during the shear-driven amorphization process. Blue spheres are Si atoms in the Si-I phase, while gray spheres are Si atoms in an amorphous configuration. The black and red circles indicate two atoms that are initially in a crystalline lattice position and are pushed into the crystal during the process, thus causing the advancement of the amorphous region. Their initial coordinate normal to the interface [in panel (b)] is indicated by the black and red solid lines.

average shear rate v/h. Furthermore, the time evolution of h in Si-I [Fig. 2(a), red line; see discussion S3 in the Supplemental Material [34] for details on the computation of h] can be fitted by the square root function

$$h(P,t) = h_0 + \sqrt{2\lambda(P)vt} \tag{1}$$

[Fig. 2(a), red dashed line], where h_0 is the initial thickness of the amorphous region, $\lambda(P)$ is a measure of amorphization rate that has units of length, and vt is the sliding distance.

This square root law is typical of a mechanically driven amorphization process, whose rate dh/dt depends on the local shear rate, $dh/dt = \lambda(P)v/h$, where $\lambda(P)$ is the pressure-dependent increase of h per 100% of accommodated strain. Equation (1) is the solution of this equation for constant sliding velocity v. Such an amorphization process does not require temperature activation but is driven by the shear rate v/h close to the amorphous/crystal (a/c) interface. Indeed, our simulations show that amorphization occurs even when the thermostat temperature is set to 0 K (the maximum temperature of the sliding interface due to viscous heating is lower than 60 K in this case). Also at 0 K, $h(t)$ can be fitted by the aforementioned square root functional form [Fig. 2(a), blue lines] and the amorphization rate is even larger than at 300 K. This is due to a recrystallization process which opposes amorphization but is suppressed at zero temperature (see discussion S4 in the Supplemental Material [34]). Finally, $h(t)$ is determined solely by the sliding distance vt. This is

confirmed by simulations performed at different sliding speeds ($v = 10,\ 20$, and $30\,\mathrm{m\,s^{-1}}$). As shown in the inset of Fig. 2(a), the three $h(t)$ curves collapse if plotted as a function of the sliding distance rather than of the sliding time. Qualitatively similar results were presented in Ref. [5] for C.

These results show that the shear-driven growth of a-Si and a-C has the same mechanical nature, but that the two crystals have opposite behavior with respect to the change in specific volume upon amorphization. Accordingly, the atomic-scale mechanisms that take place at the a/c interface and lead to the growth of the amorphous phase are reversed in Si-I and diamond. As described in detail in Ref. [5], the shear rate at the a/c interface allows C atoms in the a-C region to pull neighboring C atoms out of the denser crystal. An analysis of the MD trajectories indicates that in Si-I local shear events cause Si atoms at the a/c interface to be pushed into the crystal, thus increasing its local density, perturbing its local tetrahedral structure [Figs. 2(b)–2(e)], and eventually causing amorphization. This is reminiscent of a crystalline-to-amorphous transition observed by insertion of self-interstitial defects in Si-I [35].

The opposite sign of the volume variation of the two materials upon shear-driven amorphization should lead to a different dependence of the amorphization rate on the normal load because in Si-I (volume contracts) the external compressive force helps amorphization while in C (volume expands) it opposes it. To investigate this, we performed MD sliding simulations at 300 K and varying applied load, ranging between 5 and 15 GPa for Si-I and between 10 and 100 GPa for C. The time evolution of h for all the investigated values of the normal load is plotted in Fig. 3(a) for Si-I and in Fig. 3(b) for C (solid lines). For the cases in which recrystallization is not too pronounced (i.e., $P > 8$ GPa in Si and $P < 100$ GPa in C), the $h(t)$ curves can be fitted by Eq. (1) [Figs. 3(a) and 3(b), dashed lines] and the corresponding $\lambda(P)$ is shown in Figs. 3(c) and 3(d) (red circles). We note that at $P = 15$ GPa the Si system is very close to the melting temperature of the Si-I phase [cf. P-T diagram in Fig. 1(a), where the melt line for the Si-I phase extends into the region of stability of the kinetically hindered Si-II phase]. Here, the amorphization rate is not well fitted by a square root function, likely because of premelting that contributes to amorphization. As anticipated above, these simulations show that with increasing normal load the average amorphization rate increases in Si-I while it decreases in diamond. For Si, this is confirmed by sliding simulations at 0 K [Fig. 3(c), blue squares], where recrystallization is suppressed (discussion S4 in the Supplemental Material [34]). The pressure dependence of $\lambda(P)$ is therefore mostly due to the sign of the volume change upon amorphization rather than to the recrystallization kinetics.

As a final step, we compared density and structure of shear-induced a-Si and a-C to those of liquid phases, amorphous solids quenched at constant pressure, and hydrostatically compressed amorphous solids. The hydrostatically compressed a-Si and a-C were obtained by quasistatically compressing an amorphous system that was quenched from the liquid at constant pressure $P = 0$ (i.e., an LDA solid in the Si case). In the hydrostatically compressed a-Si, we observe an abrupt nonequilibrium transition between LDA and HDA Si. This polyamorphic transition [19] occurs close to the experimental

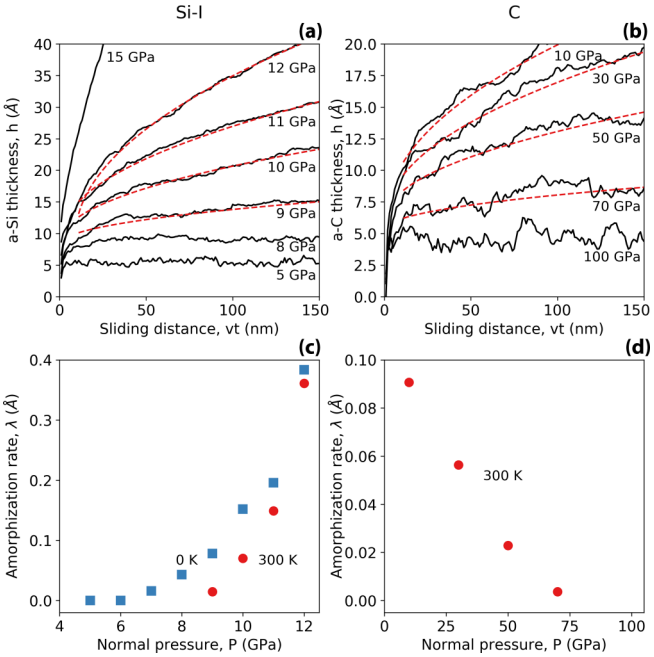

FIG. 3. (a), (b) Evolution of the amorphous region thickness h with sliding distance vt for different values of the normal pressure P for Si-I (a) and diamond (b) at 300 K. Solid lines are the h values from the MD simulations, while dashed red lines are fits to the amorphization model, Eq. (1). (c), (d) Amorphization rate λ (the increase in thickness per 100% of strain) for different values of normal pressure P for Si-I (c) and diamond (d).

LDA-HDA transition pressure of 14 GPa [18]. In contrast, shearing produces an a-Si phase that is significantly denser than Si-I and LDA Si across the whole 5–15 GPa pressure range [Fig. 1(c)]. The density of a-Si produced by shearing shows no sharp transition and closely follows the density of quenched a-Si and liquid Si. This is the HDL Si phase usually observed at $T = T_{\mathrm{m}}$ [31–33] and not the low-density liquid (LDL) whose formation is suppressed above about 5 GPa [36]. Conversely, C expands in volume across the whole pressure range [Fig. 1(d)]. The density of the sheared a-C phase is significantly lower than that of diamond and intermediate between the density of quenched a-C and liquid C. The density of hydrostatically compressed a-C is comparable to the liquid density and, since C is not known to show polyamorphic transitions [20], there is no sharp nonequilibrium transition between two a-C solids of different density.

These results are supported by an analysis of the atomic structure. Figure 4 shows the angular distribution function $g(\theta)$ (see discussion S5 in the Supplemental Material [34]) for the phases discussed above at different pressure values. Consistent with the density values shown in Fig. 1(c), quenched a-Si shows a smooth transition between the fingerprints of LDA and HDA Si [see inset in Fig. 4(b)] with increasing pressure. An analogous smooth transition is observed in a-Si obtained by shear and liquid Si at $T = T_{\mathrm{m}}$, where signatures of the HDA and HDL phases persist at low pressure. We note that the analysis of density and structure for the shear-induced a-Si was only possible for $P \gtrsim 5$ GPa, as recrystallization limits the formation of a-Si at lower pressure. Analogous plots for C confirm

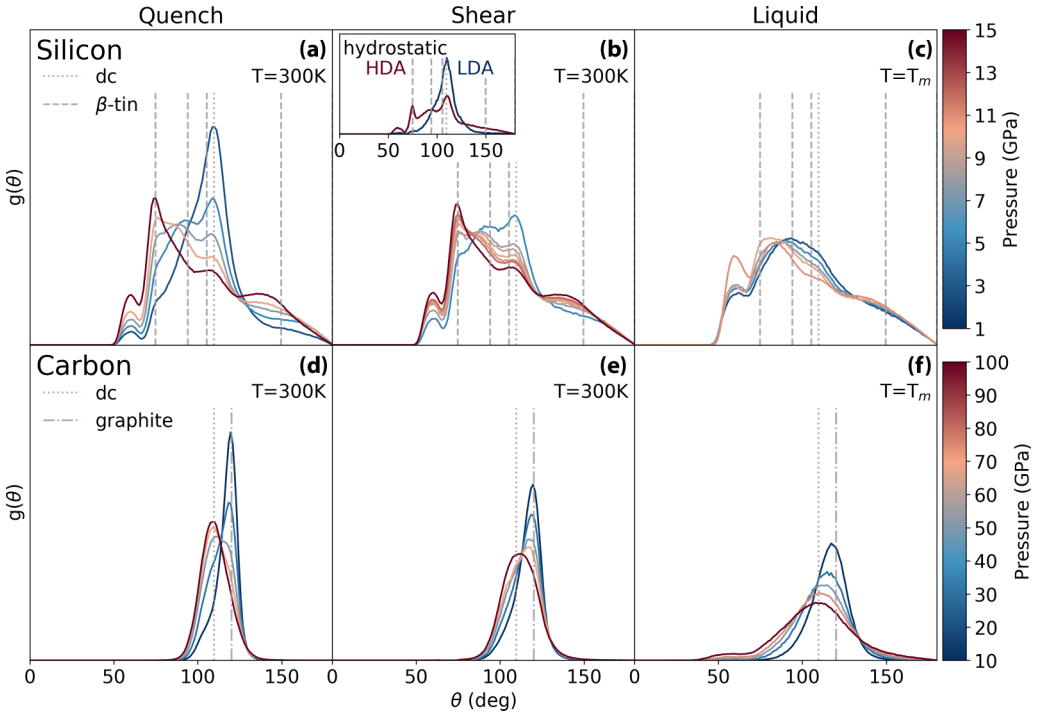

FIG. 4. Angular distribution function, $g(\theta)$, of amorphous and liquid C and Si for different pressure values. (a), (d) $g(\theta)$ for amorphous structures obtained by quenching from the melt under constant pressure. (b), (e) $g(\theta)$ for amorphous structures obtained during shear MD simulations. The inset to panel (b) shows $g(\theta)$ obtained by hydrostatic compression of Si. (c), (f) $g(\theta)$ for liquid structures at the melting point T_m. The angular distributions functions are extracted from the spatial region that is in the liquid state in the phase coexistence calculations used to compute the melting lines in Figs. 1(a) and 1(b). The vertical gray lines show the angles of the reference crystalline structures: diamond-cubic (dc) and β-tin Si, dc C, and graphite.

that the structure of a-C obtained by shearing is an intermediate between the structure of quenched a-C and liquid C.

III. DISCUSSION AND CONCLUSIONS

Our MD simulations reveal that Si-I undergoes shear-driven amorphization via a mechanical process that is analogous to the process recently discovered for diamond C crystals [5]. Shear-driven amorphization induces a densification in Si-I and a volume expansion in diamond. This is consistent with previously reported shear-induced density transitions that facilitate plastic flow in a-Si [37] and a-C [38]. The volume change upon amorphization determines whether external work is performed on or released by the system, and controls the dependency of the respective amorphization rate on pressure. Since a-Si and a-C obtained under shear are structurally similar to the respective liquid phases, the amorphization process results in shear melting. Moreover, the volume change and hence the pressure dependence of the amorphization rate can in principle be predicted by the Clausius-Clapeyron relation, i.e., by the sign of the dT_m/dP slope for the respective crystal [Figs. 1(a) and 1(b)].

Nanoscale wear of Si and C is believed to be mediated by shear-induced amorphization [5,6]. Our results indicate that, counterintuitively, the amorphization contribution to wear in diamond should decrease as the normal load increases, probably contributing to the extraordinary wear resistance of C coatings. Our observations could also be extended to a number of diamond-cubic crystals that undergo shear-driven amorphization and are particularly interesting for crystals that have a negatively sloped melting line and show polyamorphism, like Ge and H_2O. Shear-induced a-Si has HDA-like density and structure at pressures that are significantly lower than the LDA-HDA transition pressure observed under hydrostatic compression. Without this densification process shear-induced amorphization would be hindered at $P < 14$ GPa due to the fast recrystallization of the Si-I-like LDA material. Similarly to Si-I, tetrahedral ice I_h [19,20] becomes denser upon melting at ambient conditions. Its slipperiness has historically been explained by pressure melting. However, ice is slippery down to –35 °C where pressure melting is suppressed. The present understanding is that ice has a thin liquidlike surface layer, that has been linked to its friction properties [39]. Our work suggests shear-induced amorphization as a possible explanation for the formation of this layer even at low pressures and temperatures.

ACKNOWLEDGMENTS

We thank Peter Gumbsch for helpful discussions. G.M., A.K., and M.M. are grateful to Asahi Diamond Industrial Co. Ltd. for partially funding this research. L.P. acknowledges funding by the Deutsche Forschungsgemeinschaft (Grant No. PA 2023/2). Simulations were carried out on Joe at Fraunhofer IWM, on JURECA (Projects No. hfr09 and No. hfr13) at the Jülich Supercomputing Centre (JSC), and on NEMO at the University of Freiburg (DFG Grant No. INST 39/963-1 FUGG). Postprocessing and visualization were carried out with ASE [40] and OVITO [41,42].

[1] D. Hull and D. J. Bacon, *Introduction to Dislocations*, 5th ed. (Butterworth-Heinemann, Oxford, 2011).

[2] Y. He, L. Zhong, F. Fan, C. Wang, T. Zhu, and S. X. Mao, Nat. Nanotechnol. **11**, 866 (2016).

[3] J. Y. Huang, H. Yasuda, and H. Mori, Philos. Mag. Lett. **79**, 305 (1999).

[4] M. Chen, J. W. McCauley, and K. J. Hemker, Science **299**, 1563 (2003).

[5] L. Pastewka, S. Moser, P. Gumbsch, and M. Moseler, Nat. Mater. **10**, 34 (2011).

[6] X. Hu, M. V. P. Altoe, and A. Martini, Wear **370–371**, 46 (2017).

[7] B. Gotsmann and M. A. Lantz, Phys. Rev. Lett. **101**, 125501 (2008).

[8] T. D. B. Jacobs and R. W. Carpick, Nat. Nanotechnol. **8**, 108 (2013).

[9] S. Goel, A. Kovalchenko, A. Stukowski, and G. Cross, Acta Mater. **105**, 464 (2016).

[10] T. Suzuki, Y. Nishino, and J. Yan, Precis. Eng. **50**, 32 (2017).

[11] V. Domnich and Y. Gogotsi, Rev. Adv. Mater. Sci. **3**, 1 (2002).

[12] S. Jiapeng, L. Cheng, J. Han, A. Ma, and L. Fang, Sci. Rep. **7**, 10282 (2017).

[13] R. Abram, D. Chrobak, and R. Nowak, Phys. Rev. Lett. **118**, 095502 (2017).

[14] K. Minowa and K. Sumino, Phys. Rev. Lett. **69**, 320 (1992).

[15] Z. Zhang, D. Guo, B. Wang, R. Kang, and B. Zhang, Sci. Rep. **5**, 16395 (2015).

[16] S. Zhao, E. N. Hahn, B. Kad, B. A. Remington, C. E. Wehrenberg, E. M. Bringa, and M. A. Meyers, Acta Mater. **103**, 519 (2016).

[17] Y.-C. Wang, W. Zhang, L.-Y. Wang, Z. Zhuang, E. Ma, J. Li, and Z.-W. Shan, NPG Asia Mater. **8**, e291 (2016).

[18] P. F. McMillan, M. Wilson, D. Daisenberger, and D. Machon, Nat. Mater. **4**, 680 (2005).

[19] M. C. Wilding, M. Wilson, and P. F. McMillan, Chem. Soc. Rev. **35**, 964 (2006).

[20] W. Hujo, B. S. Jabes, V. K. Rana, C. Chakravarty, and V. Molinero, J. Stat. Phys. **145**, 293 (2011).

[21] B. J. Ackerson and N. A. Clark, Phys. Rev. Lett. **46**, 123 (1981).

[22] D. J. Evans, Phys. Rev. A **25**, 2788 (1982).

[23] F. P. Bundy, J. Chem. Phys. **41**, 3809 (1964).

[24] F. P. Bundy, W. A. Bassett, M. S. Weathers, R. J. Hemley, H. U. Mao, and A. F. Goncharov, Carbon **34**, 141 (1996).

[25] L. Pastewka, A. Klemenz, P. Gumbsch, and M. Moseler, Phys. Rev. B **87**, 205410 (2013).

[26] T. Kumagai, S. Izumi, S. Hara, and S. Sakai, Comput. Mater. Sci. **39**, 457 (2007).

[27] J. Tersoff, Phys. Rev. B **39**, 5566 (1989).

[28] L. Pastewka, S. Moser, and M. Moseler, Tribol. Lett. **39**, 49 (2010).

[29] E. A. J. F. Peters, Europhys. Lett. **66**, 311 (2004).

[30] W. C. Swope, H. C. Andersen, P. H. Berens, and K. R. Wilson, J. Chem. Phys. **76**, 637 (1982).

[31] D. Machon, F. Meersman, M. C. Wilding, M. Wilson, and P. F. McMillan, Prog. Mater. Sci. **61**, 216 (2014).

[32] A. Hedler, S. L. Klaumünzer, and W. Wesch, Nat. Mater. **3**, 804 (2004).

[33] S. Sastry and C. A. Angell, Nat. Mater. **2**, 739 (2003).

[34] See Supplemental Material at http://link.aps.org/supplemental/10.1103/PhysRevMaterials.2.083601 for computation of P-T phase diagrams, P dependence of Si and C density and structure, determination of amorphous regions, and preliminary simulations on Si-I recrystallization.

[35] L. Colombo and D. Maric, Europhys. Lett. **29**, 623 (1995).

[36] K. M. S. Garcez and A. Antonelli, J. Chem. Phys. **135**, 204508 (2011).

[37] M. J. Demkowicz and A. S. Argon, Phys. Rev. Lett. **93**, 025505 (2004).

[38] T. Kunze, M. Posselt, S. Gemming, G. Seifert, A. R. Konicek, R. W. Carpick, L. Pastewka, and M. Moseler, Tribol. Lett. **53**, 119 (2014).

[39] R. Rosenberg, Phys. Today **58** (12), 50 (2005).

[40] A. Larsen, J. Mortensen, J. Blomqvist, I. Castelli, R. Christensen, M. Dulak, J. Friis, M. Groves, B. Hammer, C. Hargus, E. Hermes, P. Jennings, P. Jensen, J. R. Kermode, J. Kitchin, E. Kolsbjerg, J. Kubal, K. Kaasbjerg, S. Lysgaard, J. Maronsson *et al.*, J. Phys.: Condens. Matter **29**, 273002 (2017).

[41] A. Stukowski, Modelling Simul. Mater. Sci. Eng. **18**, 015012 (2010).

[42] E. Maras, O. Trushin, A. Stukowski, T. Ala-Nissila, and H. Jonsson, Comput. Phys. Commun. **205**, 13 (2016).